A State-Space Approach to Optimal Level-Crossing Prediction for Linear Gaussian Processes

Rodney A Martin, Ph.D. *Member, IEEE*

***Abstract*— In many complex engineered systems, the ability to give an alarm prior to impending critical events is of great importance. These critical events may have varying degrees of severity, and in fact they may occur during normal system operation. In this article, we investigate approximations to theoretically optimal methods of designing alarm systems for the prediction of level-crossings by a zero-mean stationary linear dynamic system driven by Gaussian noise. An optimal alarm system is designed to elicit the fewest false alarms for a fixed detection probability. This work introduces the use of Kalman filtering in tandem with the optimal level-crossing problem. It is shown that there is a negligible loss in overall accuracy when using approximations to the theoretically optimal predictor, at the advantage of greatly reduced computational complexity.**

***Index Terms*— Optimal alarm theory, Level-crossing theory, Kalman prediction**

I. Introduction

THIS article introduces a novel approach of combining the practical appeal of Kalman filtering with the design of an optimal alarm system for the prediction of level-crossing events. A comprehensive demonstration of practical application for the design of optimal alarm systems has been covered in the literature [1], [2], [3]. However, the background theory for optimal alarm systems has seen modest coverage by other authors as well [4], [5], [6], [7]. The latter is by no means a comprehensive list, but illustrates a cross-section of the primary authors responsible for introducing optimal alarm systems in a classical and practical sense.

It was shown by Svensson [1], [2] that an optimal alarm system can be constructed by finding relevant alarm system metrics (as are used in ROC curve analysis) as a function of a design parameter by way of an optimal alarm condition. The optimal alarm condition is fundamentally an alarm region or decision boundary based upon a likelihood ratio criterion via the Neyman-Pearson lemma, as shown in [5], [6]. This allows us to design an optimal alarm system that will elicit the fewest possible false alarms for a fixed detection probability. This becomes important when considering the numerous applications that might benefit from an intelligent tradeoff between false alarms and missed detections.

Due to the fact that optimal alarm regions cannot be expressed in closed form, one of the aims of this study is to investigate approximations for the design of an optimal alarm system. The resulting metrics can easily be compared to competing methods that may also provide some level of predictive capability, but have no provision for minimizing false alarms for the prediction of level-crossing events.

There are several examples of level-crossing events to be studied, varying from a simple one-sided case to a more complicated two-sided case. The former one-sided case involves exceedances and/or upcrossings of a single level spanning two adjacent time points for a discrete-time process. This is the case that has traditionally been studied in previous work and invokes ARMA(X) prediction methods [1], [2], [4], [5], [6], [7]. The latter two-sided case involves a level crossing event that may span many time points and exceed upper and lower levels symmetric about the mean of the process many times during this timeframe.

A variant of the latter more complicated two-sided case has been investigated by Kerr [8] and uses a Kalman filter-based approach. The two-sided case is more practically relevant when monitoring residuals that may be derived from the output of other machine learning algorithms or transformed parameters that relate to system performance. We investigate the two-sided case here, and also use a Kalman filter-based approach in an optimal manner relevant for the prediction of level-crossings.

The prediction of such a level-crossing event is also very similar to what has been established as the state of the art for newly minted spacecraft engines, as studied in [9], however no guarantees of optimality exist. This provide us additional practical motivation for investigating a level crossing event that spans many time points, moving beyond what has previously been studied in this vein. In general, the design of optimal alarm systems demonstrates practical potential to enhance reliability and support health management for space propulsion, civil aerospace applications, and other related fields. Due to the great costs, not to mention potential dangers associated with a false alarm due to evasive or extreme action taken as a result of false indications, there are great opportunities for cost savings/cost avoidance, and enhancement of overall safety. Nonetheless, our intent is to demonstrate the utility of optimal level-crossing prediction from a more theoretical perspective.

There is an extensive history of invoking Kalman-filter-based approaches within the failure detection literature. A few of the most groundbreaking articles that discuss the use of Kalman filter methods for failure detection have been authored by Kerr [8], and Willsky and Jones [10]. Both of these articles have a long history of related methods descending from them, *i.e.*, [11] which alludes to the use of the Neyman-Pearson lemma. More recently, the use of the Kalman filter has been used to address the level-crossing prediction problem

Manuscript received xxx xx, 2007; revised xxx xx, 2009. This work was supported by xxxx.

Rodney A. Martin is with the NASA Ames Research Center

in application to condition monitoring [12], however without any theoretical guarantees of optimality. A competitor to the optimal alarm system is described in [13], and uses adaptive optimal on-line techniques in a Bayesian formulation, providing more modeling flexibility. However, there are still considerable computational issues with such an approach, and a well-defined cost function is still required, even when the posterior probability is adaptively updated.

One recent criticism of [10] addresses the claim of its optimality by Kerr [14]. This method, presented by Willsky and Jones, is characterized by a formulation of the failure detection problem involving the GLR (Generalized Likelihood Ratio) test. The method derived by Kerr shows how to derive a failure detection algorithm whose design is performed by computing false alarm and correct detection probabilities over a time interval. Neither method is optimal in the sense used to predict level-crossings, as introduced by DeMaré [5] and Svensson et al. [2]. Other standard methods based upon the GLR test, and SPRT (Sequential Probability Ratio Test) invoke hypothesis tests that are geared more for detection of the change of model parameters, as opposed to level-crossings.

As was previously mentioned in this section, we aim to more precisely close the gap between the use of Kalman filtering and optimal alarm systems in this article. Although this article is motivated by fault detection and prediction, and it is recognized that the literature in this area is quite expansive, our investigation aims to shed light on a segment of the literature that has been largely overlooked.

II. Performance Analysis

As mentioned previously, relevant alarm system metrics such as ones used in ROC curve analysis can be expressed as a function of a design parameter via an optimal alarm condition. These same metrics will act as the basis for comparison to competing methods that are functions of different design parameters. These competing methods may provide some level of predictive capability, but have no provision for minimizing false alarms. The two primary methods to provide a baseline for comparison are to compare the process value with a fixed threshold, or the "redline" method, and to compare future predicted process value with a fixed threshold, or the "predictive" method.

However, in both cases it is important to make the distinction between the critical level, L, associated with the level crossing event to be predicted and the fixed threshold referred to above, denoted as L_A. The critical level represents the threshold above which damage or some significant decrease in quality of a behavior or process may potentially occur. There are some cases in which this critical level, L, is not known, have not been designed *a priori*, or when known critical levels yield alarm systems that are practically infeasible. As such, sometimes it is beneficial to use values that are based upon statistical outlier detection and hypothesis testing via the p-value.

The fixed threshold, L_A, essentially acts as a design parameter with which to tune the alarm system sensitivity. Its value is the level at which an alarm would be triggered, whose selection may be performed with the aid of ROC analysis. The main utility of using two distinct levels, however, is to enable the decoupling of alarm design from construction of the critical event itself. Two levels are also often used in practice for the design of fault detection algorithms that involve limit-based abort decisions. A "yellow-line" limit check is often used as a precursor caution and warning threshold to the "redline" abort threshold. The former can be used as an alarm system design parameter, where the latter may serve as a hard limit determined apriori via extensive experimental validation.

To recap, the redline and predictive techniques both use fixed thresholds, L_A, and the optimal level-crossing predictor uses an optimal alarm condition (or approximations of it). All three techniques are leveraged to predict another distinctly more critical level-crossing event (based upon the critical level, L), and all are preferable to the use of a *single* level for a number of reasons. For one, ROC curve statistics (the true and false positive rates) can be expressed directly as a function of the model parameters when using these techniques. Therefore, design of the alarm system can proceed without the need to observe actual examples of failures, and there is no need to estimate the alarm system metrics empirically. This obviates the need to rely upon having actual available examples of failures for alarm system design to generate the ROC curve.

It is not possible to construct an ROC curve as a function of model parameters when using a single level. In this case the ROC curve statistics can only be estimated empirically with observational and truth data. Truth data in this case can either be represented by model generated level-crossing events, or failures generated from a complex system. The construction of an ROC curve in this manner can be used for any alarm system technique. However, in the absence of actual observations of failures, the "Monte-Carlo" style method of generating truth data can be computationally intensive, and is still based purely upon simulated model-generated level-crossings. As such, it is imperative that the gap between model-generated failures and actual observations of failures be made as small as possible. The level-crossing event must sufficiently characterize an actual physical failure to realize the advantage of expressing the ROC curve of as a function of the model parameters, and thus to design an alarm system without the need to observe actual examples of failures.

The redline, predictive, and optimal techniques are preferable to the use of a *single* level for another reason. The former three techniques generate ROC curve statistics that are based upon the use of distinct design spaces for construction of a critical event and their respective alarm systems, providing a measure of functional distinction. The critical event can be constructed such that multiple level-crossings span multiple time steps into the future, implicitly enabling a predictive assessment capability for alarm system design. Using a single level-based alarm system merges the functionality of limit checking and the use of an alarm design parameter. As such it is not possible to decouple independent alarm design from the critical event, and thus this method provides no measure of functional distinction. It is also the one most commonly found in the literature, *i.e.*, [15], [8], [10]. Arguably, the critical event should be constructed to emulate the physics of the failure, and

the alarm system should independently be designed to predict it. The distinction between these two paradigms is one of the most discernable differences in the theoretical techniques used here and in other literature, [1], [2], [3], [4], [5], [6].

III. Methodology

A level-crossing event is defined with a critical level, L, that is assumed to have a fixed, static value. The level is exceeded by some critical parameter than can be represented by a dynamic process, and is often modeled as a zero-mean stationary linear dynamic system driven by Gaussian noise. Most of the theory that follows is based upon this standard representation of the optimal level-crossing problem. As such, our underlying assumption is that we can fit measured or transformed data to a model represented by a linear dynamic system driven by Gaussian noise. The state-space formulation is shown in Eqns. 1-3, demonstrating propagation of both the state, $\mathbf{x}_k \in \mathbb{R}^n$ which is corrupted by process noise $\mathbf{w}_k \in \mathbb{R}^n$, and the state covariance matrix, $\mathbf{P}_k$, which evolve with the time-invariant system matrix $\mathbf{A}$. The output, $y_k \in \mathbb{R}$ is univariate, and is corrupted by measurement noise $v_k \in \mathbb{R}$.

$$\begin{aligned} \mathbf{x}_{k+1} &= \mathbf{A}\mathbf{x}_k + \mathbf{w}_k & (1)\\ y_k &= \mathbf{C}\mathbf{x}_k + v_k & (2)\\ \mathbf{P}_{k+1} &= \mathbf{A}\mathbf{P}_k\mathbf{A}^T + \mathbf{Q} & (3) \end{aligned}$$

where

$$\begin{aligned} \mathbf{w}_k &\sim \mathcal{N}(0, \mathbf{Q}), \quad \mathbf{Q} \succeq \mathbf{0}\\ v_k &\sim \mathcal{N}(0, R), \quad R > 0\\ \mathbf{x}_0 &\sim \mathcal{N}(\mu_{\mathbf{x}}, \mathbf{P}_0) \end{aligned}$$

A summary of the notation to be used henceforth is provided in Table I. As mentioned previously, there is great flexibility in constructing a mathematical representation for the level-crossing event, C_k. Ostensibly, the target application will drive the definition of this event. As such, in this paper the event of interest is shown in Eqn. 4, *cf.* Kerr [8] in consideration of the motivating factors described in the introduction. This level-crossing event represents at least one exceedance outside of the threshold envelope specified by $[-L, L]$ of the process y_k within the specified look-ahead prediction window, d.

$$C_k \triangleq \bigcup_{j=1}^{d} S_{k+j} = \bigcup_{j=1}^{d} E'_{k+j} = \mathcal{I} \setminus \bigcap_{j=1}^{d} E_{k+j} \qquad (4)$$

where

$$\begin{aligned} E_{k+j} &\triangleq \{|y_{k+j}| < L\}, \ \forall j \geq 1\\ S_{k+j} &\triangleq \begin{cases} E'_{k+j} & j = 1\\ \bigcap_{i=1}^{j-1} E_{k+i}, E'_{k+j} & \forall j > 1 \end{cases} \end{aligned}$$

Fig. 1 illustrates the relationship between subevents S_{k+j} and E_{k+j}, when $d = 5$. The event C_k can be represented as the union of disjoint subevents, S_{k+j}, or as the union of overlapping subevents, E'_{k+j}. However, due to DeMorgan's theorem, the latter can be expressed in a more compact fashion via a *single* term when computing the probability of the overall event. This obviates the need for use of the inclusion/exclusion rule for the realization of all relevant terms in a probability computation based upon the union of overlapping subevents, E'_{k+j}, where the number of terms would be exponential in d. It also obviates the need for computing the probability based upon the former union of disjoint subevents, S_{k+j}, where there is no need for use of the inclusion/exclusion rule. However, the number of terms would still be linear in d, as the probability computation of the union of disjoint subevents is represented by the sum of terms involving S_{k+j}. Thus Eqn. 5 represents the unconditional probability of the level-crossing event in its most compact representational form.

$$P(C_k) = 1 - \int_{-L}^{L} \cdots \int_{-L}^{L} \mathcal{N}(\mathbf{y}_d; \mu_{\mathbf{y}_d}, \Sigma_{\mathbf{y}_d}) d\mathbf{y}_d \qquad (5)$$

where

Mathematical Representation	*Nomenclature*
$\mu_\bullet$	$E[\bullet]$(Expectation)
$\hat{\bullet}_{k+j\|k}$	$E[\bullet\|y_0, \ldots, y_k]$ (Conditional Expectation)
$\tilde{\bullet}_k$	Orthonormal rotation of $\bullet_k$ in vector space
$\bullet^*$	Result of vector space orthonormal rotation in probability or event space
$\mathbf{P}_{k+i,k+j}$	State autocovariance matrix
$\mathbf{P}_{ss}^L$	Solution to Discrete Algebraic Lyapunov Equation
$\mathbf{P}_{ss}^R$	Solution to Discrete Algebraic Riccati Equation (*A priori* steady-state error covariance matrix)
$\hat{\mathbf{P}}_{ss}^R$	(*A posteriori* steady-state error covariance matrix)
$\mathbf{F}_{k+1\|k}$	Kalman Gain
$\mathbf{F}_{ss}$	Steady-State Kalman Gain
$V_{k+j\|k}$	Conditional prediction variance for future output value
C_k	Level-crossing event
S_{k+j}	Level-crossing subevent (disjoint)
E_{k+j}	Level-crossing subevent (non-disjoint)
$\mathcal{I}$	Universe of all events
A_k	Optimal alarm event (sublevel set)
Ω_C	Region in vector space spanned by level-crossing event
L_A	Level set for optimal alarm event *or* design threshold for "redline" and "predictive" methods
Ω_{A_j}	Sublevel set for subevent (used in root-finding approximation to optimal alarm event)
A_k^j	Sublevel set for subevent (used in closed-form approximation to optimal alarm event)
$A_k^{i,j}$	Sublevel set for decomposed subevent (used in closed-form approximation to optimal alarm event)
L_{A_j}	Level set for subevent (used in (either) approximation to optimal alarm event)
L	Critical level
d	Prediction horizon
P_b	Border Probability
$P_{b_{crit}}$	Critical Border Probability (Domain Boundary)
P_d	Detection Probability
P_{fa}	False Alarm Probability

TABLE I
SUMMARY OF MATHEMATICAL NOTATION

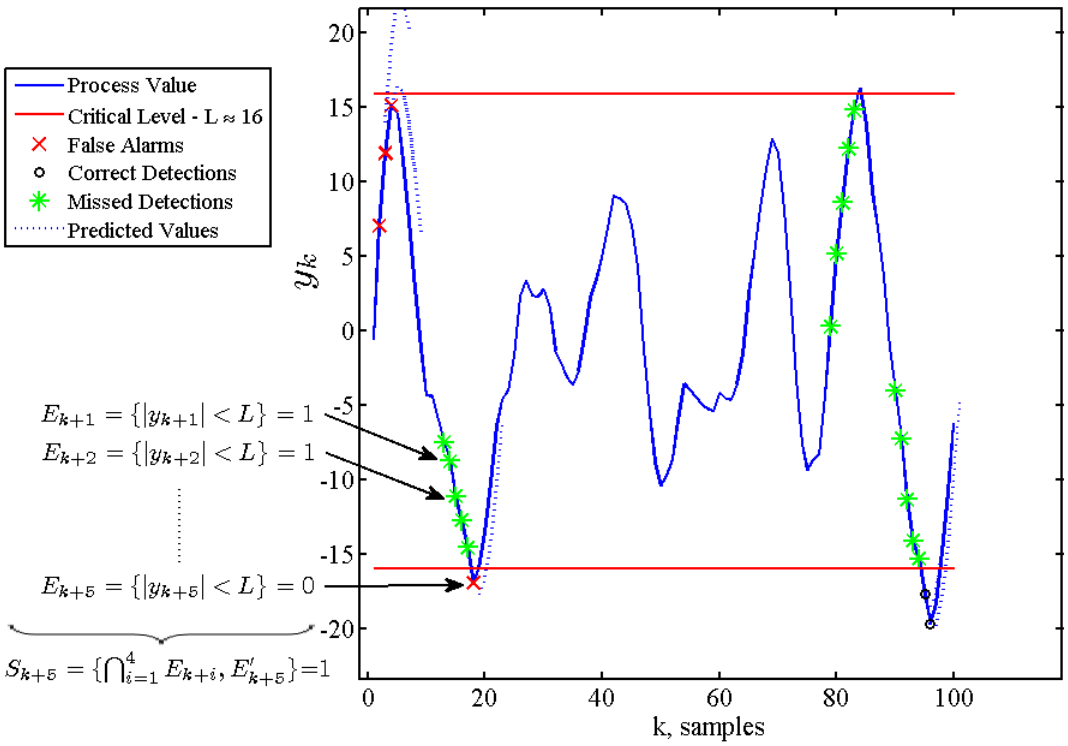

Fig. 1. Level-Crossing Event Realization

$$\mathbf{y}_d \triangleq \begin{bmatrix} y_{k+1} \\ \vdots \\ y_{k+d} \end{bmatrix}, \quad \mu_{\mathbf{y}_d} = \mathbf{0}_d = \begin{bmatrix} 0 \\ \vdots \\ 0 \end{bmatrix}$$

$$\Sigma_{\mathbf{y}_d} \triangleq \begin{cases} \mathbf{C}\mathbf{P}_k\mathbf{C}^\top + R & \forall i = j \in [1,\ldots,d] \\ \mathbf{C}\mathbf{P}_{k+i,k+j}\mathbf{C}^\top & \forall j > i \in [1,\ldots,d] \end{cases}$$

$$\text{and } \mathbf{P}_{k+i,k+j} \triangleq \mathbf{A}^j(\mathbf{P}_k - \mathbf{P}_{ss}^L)(\mathbf{A}^\top)^i + \mathbf{A}^{j-i}\mathbf{P}_{ss}^L$$

We may approximate $\Sigma_{\mathbf{y}_d}$ as shown in Eqn. 6 by substituting the steady-state version of the Lyapunov equation given previously as Eqn. 3, $\mathbf{P}_{ss}^L$, in place of $\mathbf{P}_k$, which agrees with our assumption of stationarity.

$$\Sigma_{\mathbf{y}_d} \approx \begin{cases} \mathbf{C}\mathbf{P}_{ss}^L\mathbf{C}^\top + R & \forall i = j \in [1,\ldots,d] \\ \mathbf{C}\mathbf{A}^{j-i}\mathbf{P}_{ss}^L\mathbf{C}^\top & \forall j > i \in [1,\ldots,d] \end{cases} \quad (6)$$

This approximation, while it introduces error with regards to the probability of a level-crossing event, $P(C_k)$ at a specific point in time, k, is ostensibly negligible and will provide for a great computational advantage in the design of all alarm systems that it is based upon. Instead of designing an optimal alarm system for each time step, we design a single alarm system based upon the limiting statistics that are reached at steady-state, greatly reducing the computational burden. The steady-state assumption has not been used in work by Antunes *et al.* [13], but doing so also incurs much greater computational effort.

Theorem 1, which can be found in Appendix I, provides the mathematical underpinnings for the optimal alarm condition corresponding to the level-crossing event, shown here as Eqn. 7. Alternatively, the optimal alarm condition derived in Theorem 1 can be expressed in terms of the subevents E_{k+j}, as shown in Eqn. 8.

$$P(C_k|y_0,\ldots,y_k) \geq P_b \quad (7)$$

$$\Leftrightarrow P(\bigcap_{j=1}^{d} E_{k+j}|y_0,\ldots,y_k) \leq 1 - P_b \quad (8)$$

The optimal alarm condition has therefore been derived from the use of the likelihood ratio resulting in the conditional inequality as given in Eqn. 7. This basically says "give alarm when the conditional probability of the event, C_k, exceeds the level P_b." Here, P_b represents some optimally chosen border or threshold probability with respect to a relevant alarm system metric. It is necessary to find the alarm regions in order to design the alarm system. This alarm region is parameterized by future process output predictions and covariances, which can be derived from standard Kalman filter Eqns. 9 - 13.

$$\hat{y}_{k|k} = \mathbf{C}\hat{\mathbf{x}}_{k|k} \quad (9)$$
$$\hat{\mathbf{x}}_{k+1|k} = \mathbf{A}\hat{\mathbf{x}}_{k|k} \quad (10)$$
$$\mathbf{F}_{k+1|k} \triangleq \mathbf{P}_{k+1|k}\mathbf{C}^T(\mathbf{C}\mathbf{P}_{k+1|k}\mathbf{C}^T + R)^{-1} \quad (11)$$
$$\mathbf{P}_{k+1|k} = \mathbf{A}\mathbf{P}_{k|k}\mathbf{A}^T + \mathbf{Q} \quad (12)$$
$$\mathbf{P}_{k+1|k+1} = \mathbf{P}_{k+1|k} - \mathbf{F}_{k+1|k}\mathbf{C}\mathbf{P}_{k+1|k} \quad (13)$$

where

$$\hat{\mathbf{x}}_{k|k} \triangleq E[\mathbf{x}_k|y_0,\ldots,y_k]$$
$$\mathbf{P}_{k|k} \triangleq E[(\mathbf{x}_k - \hat{\mathbf{x}}_{k|k})(\mathbf{x}_k - \hat{\mathbf{x}}_{k|k})^T|y_0,\ldots,y_k]$$

Relevant predictions, covariances and cross-covariances are given below as Eqns. 14- 18, respectively.

$$\hat{y}_{k+j|k} = \mathbf{C}\mathbf{A}^j\hat{\mathbf{x}}_{k+j|k} \quad (14)$$
$$\mathbf{P}_{k+j|k} = \mathbf{A}^j(\mathbf{P}_{k|k} - \mathbf{P}^L_{ss})(\mathbf{A}^\top)^j + \mathbf{P}^L_{ss} \quad (15)$$
$$\approx \mathbf{A}^j(\hat{\mathbf{P}}^R_{ss} - \mathbf{P}^L_{ss})(\mathbf{A}^\top)^j + \mathbf{P}^L_{ss} \quad (16)$$
$$\mathbf{P}_{k+i,k+j|k} = \mathbf{A}^j(\mathbf{P}_{k|k} - \mathbf{P}^L_{ss})(\mathbf{A}^\top)^i + \mathbf{A}^{j-i}\mathbf{P}^L_{ss} \quad (17)$$
$$\approx \mathbf{A}^j(\hat{\mathbf{P}}^R_{ss} - \mathbf{P}^L_{ss})(\mathbf{A}^\top)^i + \mathbf{A}^{j-i}\mathbf{P}^L_{ss} \quad (18)$$
$$\hat{\mathbf{P}}^R_{ss} = \mathbf{P}^R_{ss} - \mathbf{F}_{ss}\mathbf{C}\mathbf{P}^R_{ss} \quad (19)$$
$$\mathbf{F}_{ss} = \mathbf{P}^R_{ss}\mathbf{C}^T(\mathbf{C}\mathbf{P}^R_{ss}\mathbf{C}^T + R)^{-1} \quad (20)$$

$\mathbf{P}^R_{ss}$ is the combined steady-state version of Eqns. 12 and 13 given previously, or the discrete algebraic Riccati equation, and $\hat{\mathbf{P}}^R_{ss}$ is the steady-state *a posteriori* covariance matrix given in Eqn. 19. Eqn. 20 is also used in Eqn. 19, which is the steady-state version of the Kalman gain from Eqn. 11.

The approximations shown in Eqns. 16 and 18 will provide for a great computational advantage in design of the optimal alarm system and its corresponding approximations for reasons stated previously. Due to the approximation of $\mathbf{P}_{k|k}$ with $\hat{\mathbf{P}}^R_{ss}$ shown in these equations, the Kalman filter will be suboptimal, as cited by Lewis [16]. However, the assumption of stationarity is required for the design of an optimal alarm system as defined by Theorem 1, and holds here as well.

A more formal representation of the optimal alarm region is shown in Eqn. 21, which essentially defines a sublevel set of $g(\hat{\mathbf{y}}_d) \triangleq P(\bigcap_{j=1}^d E_{k+j}|y_0,\ldots,y_k)$ as a function of $\hat{\mathbf{y}}_d$.

$$A_k \triangleq \{\bigcap_{i=1}^d \hat{y}_{k+i|k} : P(C_k|y_0,\ldots,y_k) \geq P_b\} \quad (21)$$
$$\triangleq \{\bigcap_{i=1}^d \hat{y}_{k+i|k} : P(\bigcap_{j=1}^d E_{k+j}|y_0,\ldots,y_k) \leq 1 - P_b\}$$

Eqns. 22-23 give the multivariate normal probability computation to be performed via numerical integration, required for enabling the optimal alarm condition.

$$P(\bigcap_{j=1}^d E_{k+j}|y_0,\ldots,y_k) = \int_{-L}^{L}\cdots\int_{-L}^{L}\mathcal{N}(\mathbf{y}_d;\hat{\mathbf{y}}_d,\hat{\Sigma}_{\mathbf{y}_d})d\mathbf{y}_d \quad (22)$$

$$= \int_{-L-\hat{y}_{k+1|k}}^{L-\hat{y}_{k+1|k}}\cdots\int_{-L-\hat{y}_{k+d|k}}^{L-\hat{y}_{k+d|k}}\mathcal{N}(\mathbf{y}_d;\mathbf{0}_d,\hat{\Sigma}_{\mathbf{y}_d})d\mathbf{y}_d \quad (23)$$

where

$$\hat{\mathbf{y}}_d \triangleq E[\mathbf{y}_d|y_0,\ldots,y_k] = \begin{bmatrix}\hat{y}_{k+1|k}\\ \vdots \\ \hat{y}_{k+d|k}\end{bmatrix}$$
$$\hat{\Sigma}_{\mathbf{y}_d} \triangleq \begin{cases} V_{k+i|k} & \forall i = j \in [1,\ldots,d] \\ \mathbf{C}\mathbf{P}_{k+i,k+j|k}\mathbf{C}^\top & \forall i \neq j \in [1,\ldots,d]\end{cases}$$
$$V_{k+i|k} \triangleq \mathbf{C}\mathbf{P}_{k+i|k}\mathbf{C}^\top + R$$

The feasible region for values of P_b can easily be determined by applying an intermediate value theorem from calculus which provides sufficient conditions for finding a level set solution. The sufficient conditions are shown as Eqns. 24-25, and the resulting level set is shown as Eqn. 26.

$$g(\mathbf{0}_d) \geq 1 - P_b \quad (24)$$
$$\lim_{|\hat{\mathbf{y}}_d|\setminus\hat{y}_{k+j|k}\to\infty} g(\hat{\mathbf{y}}_d) < 1 - P_b, \quad \forall j \in [1,\ldots,d] \quad (25)$$

$$L_A \triangleq \{\bigcap_{j=1}^d \hat{y}_{k+j|k} : g(\hat{\mathbf{y}}_d) = 1 - P_b\} \quad (26)$$

The notation that represents the limiting condition shown in Eqn. 25 is $|\hat{\mathbf{y}}_d|\setminus\hat{y}_{k+j|k} \to \infty$, and is meant to indicate that all elements of $\hat{\mathbf{y}}_d$ other than $\hat{y}_{k+j|k}$ approach $\pm\infty$. Application of this condition yields $P_b < 1$, which is true by definition, and application of the sufficient condition shown in Eqn. 24 yields $P_b \geq 1 - g(\mathbf{0}_d)$. Thus the feasible region for P_b is $P_b \in [1 - g(\mathbf{0}_d), 1]$.

It is not possible to obtain a closed-form representation of the parametrization for the optimal alarm region shown in Eqn. 21. As such, resulting ROC curve statistics can not be computed analytically by means of numerical integration as will be shown to be possible for other methods. As an alternative, we must use the Monte Carlo style approach discussed previously. This will alow for the ROC curve statistics to be estimated empirically with observational and truth data generated from the existing model and corresponding simulations of level-crossing events.

However, as will be shown, with the aid of two distinct approximations we can generate ROC curve statistics by numerically integrating expressions for the computation of relevant multivariate normal probabilities. These multivariate probability computations are performed by using an adaptation of Genz's algorithm [17], which is based upon a robust and computationally efficient technique designed to be used for integrations in multiple dimensions for multivariate normal distributions. This provides a tool necessary for the design of approximations to an optimal alarm system, and also other failure detection algorithms such as the one most often used by Kerr [18], who specifically cites issues with the computation of these types of integrals. As such, we can avoid otherwise often very time and computationally intensive simulation runs when using Monte-Carlo style empirical estimation.

A. Root-finding Approximation

The optimal alarm region, A_k, can be approximated by the alarm region specified by $\bigcup_{j=1}^{d} \Omega_{A_j}$. Fundamentally, the approximation is constructed by solving for asymptotic bounds on the exact alarm region. By using asymptotes, we are implicitly making a geometrical approximation by forming a hyperbox around the alarm region. Simple 2-dimensional examples of such hyperboxes for various values of L, and P_b are shown in Fig. 2. There is visual evidence that limiting effects for this approximation exist, as both L and P_b approach the extremities of their feasible ranges. These effects will be touched on briefly later in the results section, but will be investigated in earnest in a sequel article.

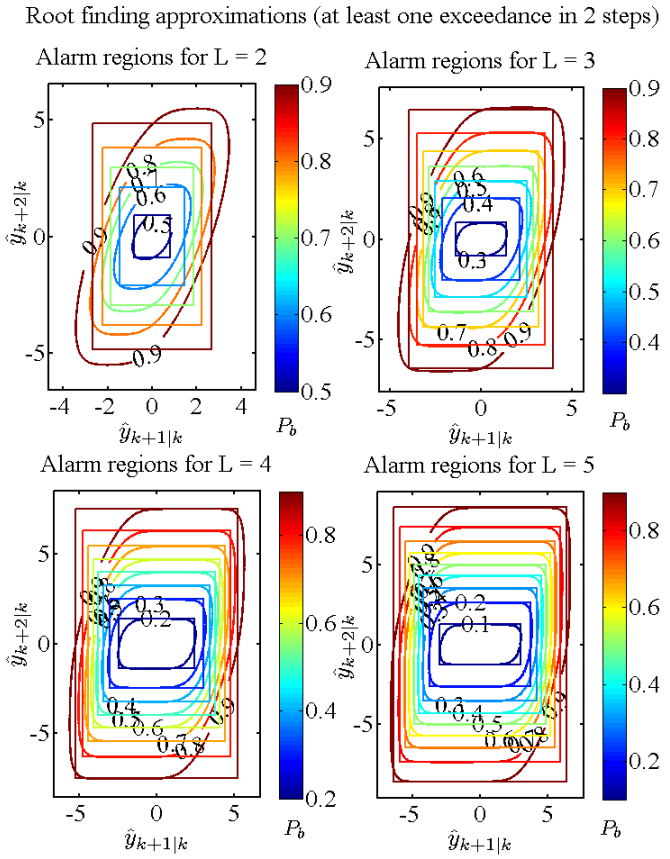

Fig. 2. Root-finding approximations for optimal alarm region

Mathematically, the approximation is formed by solving a root-finding problem which yield bounding asymptotes. The root-finding problem is posed by first taking the limit as each dimension of Eqn. 21 approaches 0, other than the one for which the asymptote is being derived. Eqn. 27 expresses this limiting condition as a function of the dimension of interest.

$$f(\hat{y}_{k+j|k}) \triangleq \lim_{\hat{\mathbf{y}}_d \setminus \hat{y}_{k+j|k} \to 0} P(\bigcap_{j=1}^{d} E_{k+j} | y_0, \ldots, y_k) \tag{27}$$

Having defined $f(\hat{y}_{k+j|k})$, it is now possible to express Ω_{A_j} by Eqns. 28-29.

$$\begin{aligned} \Omega_{A_j} &= \{\hat{y}_{k+j|k} : f(\hat{y}_{k+j|k}) \leq 1 - P_b\} && (28) \\ &= \{|\hat{y}_{k+j|k}| \geq L_{A_j}\} && (29) \end{aligned}$$

where the root-finding problem is given by numerically solving Eqn. 30.

$$L_{A_j} \triangleq \{|\hat{y}_{k+j|k}| : f(\hat{y}_{k+j|k}) = 1 - P_b\} \tag{30}$$

Thus the root-finding approximation to the optimal alarm region is given by $\bigcup_{j=1}^{d} \Omega_{A_j} \approx A_k$. Note that the function f incorporates all elements of the covariance matrix $\hat{\Sigma}_{\mathbf{y}_d}$ when computing the asymptotes, just as when constructing the sub-level set for the the exact optimal alarm region. Furthermore, the feasible region for P_b is identical to the sublevel set of the exact optimal alarm region, $P_b \in [1 - g(\mathbf{0}_d), 1] \equiv [1 - f(0), 1]$ by using a similar argument and set of sufficient conditions, as shown in Eqns. 31-32 below.

$$\begin{aligned} f(0) &\geq 1 - P_b && (31) \\ \lim_{|\hat{y}_{k+j|k}| \to \infty} f(\hat{y}_{k+j|k}) &< 1 - P_b && (32) \end{aligned}$$

However, there is one primary difference between this approximation and exact alarm region. As far as the conditional mean, $\hat{\mathbf{y}}_d$, is concerned, the asymptotic approximation is parameterized only by the corresponding dimension of the conditional mean, $\hat{y}_{k+j|k}$. The exact optimal alarm region uses all dimensions of the distribution and thus the conditional mean, $\hat{\mathbf{y}}_d$, simultaneously.

It is possible to generate formulae for the true and false positive rates as a function of L_{A_j} by appealing to Eqns. 33-34, where in place of A_k its approximation $\bigcup_{j=1}^{d} \Omega_{A_j}$ may be used.

True positive rate:

$$P_d = P(C_k | A_k) = \frac{P(C_k, A_k)}{P(A_k)} \tag{33}$$

False positive rate:

$$\begin{aligned} P_{fa} = P(A_k | C_k') &= \frac{P(C_k', A_k)}{P(C_k')} && (34) \\ &= \frac{P(A_k) - P(C_k, A_k)}{1 - P(C_k)} \end{aligned}$$

Because we have already introduced the formula for $P(C_k)$ in Eqn. 5, which holds regardless of the alarm system being used, we must only find expressions for $P(C_k, A_k)$ and $P(A_k)$. They are given in Eqns. 35-36, where $P_{b_{crit}} \triangleq 1 - g(\mathbf{0}_d) = 1 - f(0)$, and they are also implicitly expressed as a function of the design parameter, P_b, as a consequence of Eqn. 30. Note also that the off-diagonal blocks of the covariance matrix $\Sigma_{\mathbf{z}}$ are equivalent to $\hat{\Sigma}_{\hat{\mathbf{y}}_d}$ as a consequence of the projection theorem.

$$P(A_k) = \begin{cases} P(\bigcup_{j=1}^{d} \Omega_{A_j}) & P_b > P_{b_{crit}} \\ 1 & P_b \leq P_{b_{crit}} \end{cases} \quad (35)$$
$$= \begin{cases} 1 - P(\bigcap_{j=1}^{d} \Omega'_{A_j}) & P_b > P_{b_{crit}} \\ 1 & P_b \leq P_{b_{crit}} \end{cases}$$

$$P(C_k, A_k) = \begin{cases} P(C_k) - P(A'_k) + P(C'_k, A'_k) & P_b > P_{b_{crit}} \\ P(C_k) & P_b \leq P_{b_{crit}} \end{cases} \quad (36)$$

where

$$P(A'_k) = P(\bigcap_{j=1}^{d} \Omega'_{A_j}) = P(\bigcap_{j=1}^{d} |\hat{y}_{k+j|k}| < L_{A_j})$$
$$= \int_{-L_{A_1}}^{L_{A_1}} \cdots \int_{-L_{A_d}}^{L_{A_d}} \mathcal{N}(\hat{\mathbf{y}}_d; \mu_{\mathbf{y}_d}, \hat{\Sigma}_{\hat{\mathbf{y}}_d}) d\mathbf{y}_d$$

and

$$\begin{aligned} \hat{\Sigma}_{\hat{\mathbf{y}}_d} &\triangleq \Sigma_{\mathbf{y}_d} - \hat{\Sigma}_{\mathbf{y}_d} \\ &= \mathbf{O}(\mathbf{P}_{ss}^{L} - \hat{\mathbf{P}}_{ss}^{R})\mathbf{O}^{\top} \\ \mathbf{O} &\triangleq \begin{bmatrix} \mathbf{CA} \\ \vdots \\ \mathbf{CA}^d \end{bmatrix} \end{aligned}$$

Furthermore,

$$P(C'_k, A'_k) = P(\bigcap_{j=1}^{d} E_{k+j}, \bigcap_{j=1}^{d} \Omega'_{A_j})$$
$$= \int_{-L}^{L} \cdots \int_{-L}^{L} \int_{-L_{A_1}}^{L_{A_1}} \cdots \int_{-L_{A_d}}^{L_{A_d}} \mathcal{N}(\mathbf{z}; \mu_{\mathbf{z}}, \Sigma_{\mathbf{z}}) d\mathbf{z}$$

where

$$\begin{aligned} \mathbf{z} &\triangleq \begin{bmatrix} \mathbf{y}_d \\ \hat{\mathbf{y}}_d \end{bmatrix} \\ \mu_{\mathbf{z}} &\triangleq \begin{bmatrix} \mu_{\mathbf{y}_d} \\ \mu_{\mathbf{y}_d} \end{bmatrix} \\ \Sigma_{\mathbf{z}} &\triangleq \begin{bmatrix} \Sigma_{\mathbf{y}_d} & \hat{\Sigma}_{\hat{\mathbf{y}}_d} \\ \hat{\Sigma}_{\hat{\mathbf{y}}_d} & \hat{\Sigma}_{\hat{\mathbf{y}}_d} \end{bmatrix} \end{aligned}$$

B. Closed-form Approximation

The optimal alarm region, A_k, can also be approximated by an alarm region specified by $\bigcup_{j=1}^{d} A_k^j$, with a successive approximation on A_k^j; A_k^j is defined in Eqn. 37. Fundamentally, the approximation can be constructed in the same fashion as the root-finding method, by solving for asymptotic bounds on the exact alarm region.

$$A_k^j = \{\hat{y}_{k+j|k} : P(E_{k+j}|y_0, \ldots, y_k) \leq 1 - P_b\} \quad (37)$$

A containment relationship between the exact optimal alarm region and the union of inequalities $\bigcup_{j=1}^{d} A_k^j \subseteq A_k$ can easily be shown with a linear transformation of the conditionally defined Gaussian vector $\mathbf{y}_d$ to a vector of independent variables. The integrand of Eqn. 23 is a multivariate Gaussian density whose conditional covariance matrix is given by $\hat{\Sigma}_{\mathbf{y}_d}$. The orthonormal decomposition of this covariance matrix and density of the corresponding transformed vector $\tilde{\mathbf{y}}_d$ are shown in Eqns. 38 - 40.

$$\tilde{\mathbf{y}}_d = \Lambda \mathbf{y}_d \quad (38)$$
$$\hat{\Sigma}_{\mathbf{y}_d} = \Lambda \Gamma \Lambda^{\top} \quad (39)$$
$$\mathcal{N}(\mathbf{y}_d; \mathbf{0}_d, \hat{\Sigma}_{\mathbf{y}_d}) = \mathcal{N}(\tilde{\mathbf{y}}_d; \mathbf{0}_d, \Gamma) \quad (40)$$

Here, the elements of $\tilde{\mathbf{y}}_d$ are independent, and thus Γ is diagonal. As such, geometric containment easily follows when considering a revised expression for A_k and $\bigcup_{j=1}^{d} A_k^j$. Thus, the latter approximation to the exact alarm region can be rewritten in the transformed probability space as shown in Eqn. 41. The superscript $*$ for all probabilities included in this expression refers to the transformed values that results after the orthonormal rotation. Note that this expression does not change significantly from what was given in Eqn. 37.

$$\bigcup_{j=1}^{d} A_k^j = \bigcup_{j=1}^{d} \{\hat{y}_{k+j|k} : P(E_{k+j}^* | \tilde{y}_0, \ldots, \tilde{y}_k) \leq 1 - P_b^*\} \quad (41)$$

The exact alarm region A_k can be rewritten in the transformed probability space as shown in Eqn. 42, however the expression changes significantly, and in such a manner to allow for direct comparison to Eqn. 41.

$$A_k = \{\bigcap_{i=1}^{d} \hat{y}_{k+i|k} : P(\bigcap_{j=1}^{d} E_{k+j}^* | \tilde{y}_0, \ldots, \tilde{y}_k) \leq 1 - P_b^*\}$$
$$= \{\bigcap_{i=1}^{d} \hat{y}_{k+i|k} : \prod_{j=1}^{d} P(E_{k+j}^* | \tilde{y}_0, \ldots, \tilde{y}_k) \leq 1 - P_b^*\} \quad (42)$$

Because containment in this probability space is invariant under orthonormal rotations, it follows from Eqns. 41- 42, that $\bigcup_{j=1}^{d} A_k^j \subseteq A_k$, so that the approximate alarm region is a proper subset of the exact alarm region. Fig. 3 provides illustrative evidence of this containment in the transformed probability space when $d = 2$. Here, the union of the red and blue colored sections represents A_k (formula shown below) and the blue colored section represents the approximation $A_k^1 \cup A_k^2$.

$$\begin{aligned} A_k = \{&(\tilde{y}_{k+1|k}, \tilde{y}_{k+2|k}) : P(E_{k+1}^* | \tilde{y}_0, \ldots, \tilde{y}_k) \cdot \\ &P(E_{k+2}^* | \tilde{y}_0, \ldots, \tilde{y}_k) \leq 1 - P_b^*\} \end{aligned}$$

A successive approximation is required in order to obtain a closed-form representation and parametrization of the alarm region without having to resort to root-finding required for solving $P(E_{k+j}|y_0, \ldots, y_k) \leq 1 - P_b$, which is equivalent to $P(|y_{k+j}| > L|y_0, \ldots, y_k) \geq P_b$. This second approximation is given by Eqn. 43, which breaks this condition containing an absolute value into constitutive inequalities.

$$A_k^{i,j} = \{\hat{y}_{k+j|k} : P(E_{k+j}^{i'} | y_0, \ldots, y_k) \geq P_b\} \quad (43)$$

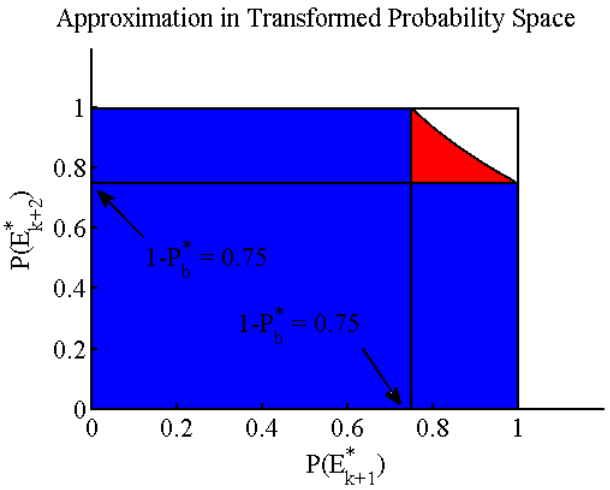

Fig. 3. Containment of the approximation by exact alarm region

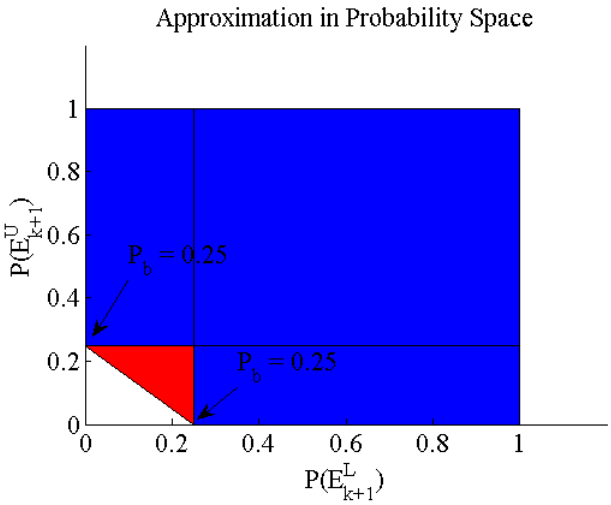

Fig. 4. Closed-form approximation in probability space

where

$$\begin{aligned} i &\in \mathcal{B} \equiv \{L, U\} \\ E^U_{k+j} &= \{y_{k+j} < L\} \\ E^L_{k+j} &= \{y_{k+j} > -L\} \end{aligned}$$

Thus $P(E^{U'}_{k+j}|y_0, \ldots, y_k) + P(E^{L'}_{k+j}|y_0, \ldots, y_k) \geq P_b$ is approximated by two distinct inequalities given by the union of $P(E^{U'}_{k+j}|y_0, \ldots, y_k) \geq P_b$ and $P(E^{L'}_{k+j}|y_0, \ldots, y_k) \geq P_b$. This subsequent approximation can easily be visualized in Fig. 4. The union of the red and blue colored sections shown in Fig. 4, represents A^1_k. Thus the blue colored section alone from Fig. 4 is a subset of this area, such that $A^{U,1}_k \cup A^{L,1}_k \subseteq A^1_k$. If we replicate Fig. 4 for $j \in [1, \ldots, d]$, then it becomes clear that more generally Eqn. 44 holds, which summarizes all of the containment relationships for the approximations covered in this subsection.

$$\bigcup_{j=1}^{d} \bigcup_{i \in \mathcal{B}} A^{i,j}_k \subseteq \bigcup_{j=1}^{d} A^j_k \subseteq A_k \tag{44}$$

By using this successive approximation, we can now represent the alarm region in "closed-form," as shown in Eqn. 45 below.

$$\bigcup_{j=1}^{d} \bigcup_{i \in \mathcal{B}} A^{i,j}_k = \bigcup_{j=1}^{d} |\hat{y}_{k+j|k}| \geq L + \sqrt{V_{k+j|k}}\Phi^{-1}(P_b) \equiv L_{A_j} \tag{45}$$

$\Phi^{-1}(\cdot)$ represents the inverse cumulative normal standard distribution function, and $L_{A_j} \forall j \in [1, \ldots, d]$ represent the limits of integration. The L_{A_j} values can now been re-defined to replace the integration limits used for the root-finding method in Eqns. 33 - 36. As such, these same equations are valid for computing P_d and P_{fa} in order to construct an ROC curve using this "closed-form" approximation as well. However, in place of A_k when using these equations, the approximation $\bigcup_{j=1}^{d} \bigcup_{i \in \mathcal{B}} A^{i,j}_k$ is used.

The domain of feasibility for this approximation now changes, and $P_{b_{crit}}$ takes on a new value, which differs from identical values of $P_{b_{crit}} = 1 - g(\mathbf{0}_d)$ and $P_{b_{crit}} = 1 - f(0)$ corresponding to the feasibility regions for the optimal alarm region and the root-finding approximation, respectively. A derivation for the new value of $P_{b_{crit}}$ is provided in Eqns. 46-50 below. The derivation is based upon the premise that $L_{A_j} > 0$, where the last step from Eqn. 49 to 50 uses Lemmas 2-5 which can be found in Appendix I, and the fact that $R > 0$.

$$\begin{aligned} L_{A_j} &> 0 \quad \forall j \in [1, \ldots, d] && (46) \\ L + \sqrt{V_{k+j|k}}\Phi^{-1}(P_b) &> 0 \quad \forall j \in [1, \ldots, d] && (47) \\ \bigcap_{j=1}^{d} P_b &> \Phi\left(\frac{-L}{\sqrt{V_{k+j|k}}}\right) \triangleq P_{b_j} && (48) \\ P_{b_{crit}} &> \max_j P_{b_j} && (49) \\ &= \Phi\left(\frac{-L}{\sqrt{V_{k+d|k}}}\right) = P_{b_d} && (50) \end{aligned}$$

Again, by using asymptotes we implicitly make a geometrical approximation by forming a hyperbox around the alarm region. As before, simple 2-dimensional examples of such hyperboxes for various values of L, and P_b are shown in Fig. 5. Furthermore, just as for the root-finding approximation, visual evidence that limiting effects for this approximation also exist, as both L and P_b approach the extremities of their feasible ranges. Note that both the approximation represented by Fig. 3 and the successive approximation represented by Fig. 4 have been applied to yield the vector space result shown in Fig. 5. Both Figs. 3 and 5 have been illustrated for the case when $d = 2$.

Due to the containment relationship labeled Eqn. 44, qualitative arguments for the under-reporting of P_d and P_{fa} can be made for this approximation. A less aggressive, more optimistic strategy will result in comparison to the exact optimal method. It is unclear if this approximation will be more or less accurate than the previous root-finding approximation.

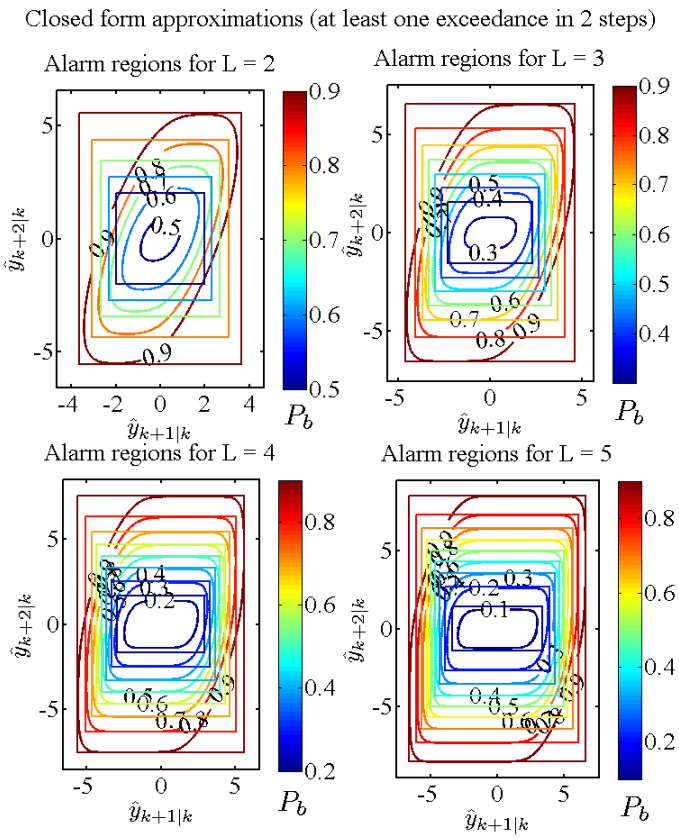

Fig. 5. Closed-form approximations for optimal alarm region

However, we do know that the off-diagonal elements of the covariance matrix $\hat{\Sigma}_{\mathbf{y}_d}$ are not used for computing the asymptotes of this "closed-form" approximation. Recall that the root-finding method incorporates all elements of the covariance matrix when computing the asymptotes. Yet both methods use asymptotic approximations which are parameterized only by the corresponding dimension of the conditional mean, $\hat{y}_{k+j|k}$.

As is apparent intuitively from Figs. 2 and 5, $A_k^j \subseteq \Omega_{A_j}$, thus $\bigcup_{j=1}^d A_k^j \subseteq \bigcup_{j=1}^d \Omega_{A_j}$. It is clear from visual comparison of these figures that this containment relationship exists between the root-finding and "closed-form" approximations. For a mathematical proof of this containment, recall Eqns. 28-29 for Ω_{A_j}, shown again below, and compare them to Eqn. 37 for A_k^j, also shown again below.

$$\begin{aligned}\Omega_{A_j} &= \{\hat{y}_{k+j|k} : f(\hat{y}_{k+j|k}) \leq 1 - P_b\} \\ &= \{|\hat{y}_{k+j|k}| \geq L_{A_j}\} \\ A_k^j &= \{\hat{y}_{k+j|k} : P(E_{k+j}|y_0, \ldots, y_k) \leq 1 - P_b\}\end{aligned}$$

If we look closely at the regions of integration for $f(\hat{y}_{k+j|k})$ and $P(E_{k+j}|y_0, \ldots, y_k)$, as shown in Eqns. 51-55 below, we will notice that a clear containment relationship exists.

$$f(\hat{y}_{k+j|k}) = \lim_{\hat{\mathbf{y}}_d \setminus \hat{y}_{k+j|k} \to 0} P(\bigcap_{j=1}^{d} E_{k+j}|y_0, \ldots, y_k) \quad (51)$$

$$= \int_{\mathcal{D}_\Omega} \mathcal{N}(\mathbf{y}_d; \hat{\mathbf{y}}_d, \hat{\Sigma}_{\mathbf{y}_d}) d\mathbf{y}_d \quad (52)$$

$$= \int_{-L}^{L} \cdots \int_{-L-\hat{y}_{k+j|k}}^{L-\hat{y}_{k+j|k}} \cdots \int_{-L}^{L} \mathcal{N}(\mathbf{y}_d; \hat{\mathbf{y}}_d, \hat{\Sigma}_{\mathbf{y}_d}) d\mathbf{y}_d \quad (53)$$

$$P(E_{k+j}|y_0, \ldots, y_k) = \int_{\mathcal{D}_A} \mathcal{N}(\mathbf{y}_d; \hat{\mathbf{y}}_d, \hat{\Sigma}_{\mathbf{y}_d}) d\mathbf{y}_d \quad (54)$$

$$= \int_{-\infty}^{\infty} \cdots \int_{-L-\hat{y}_{k+j|k}}^{L-\hat{y}_{k+j|k}} \cdots \int_{-\infty}^{\infty} \mathcal{N}(\mathbf{y}_d; \hat{\mathbf{y}}_d, \hat{\Sigma}_{\mathbf{y}_d}) d\mathbf{y}_d \quad (55)$$

where

$$\begin{aligned}\mathbb{X} &= \{[-L, L]\} \subset \mathbb{R} \\ \mathcal{D}_\Omega &= \{\mathbb{X}^{d-1} \times [-L - \hat{y}_{k+j|k}, L - \hat{y}_{k+j|k}]\} \\ \mathcal{D}_A &= \{\mathbb{R}^{d-1} \times [-L - \hat{y}_{k+j|k}, L - \hat{y}_{k+j|k}]\}\end{aligned}$$

It is clear that $\mathcal{D}_\Omega \subseteq \mathcal{D}_A$ due to the fact that $\mathbb{X}^{d-1} \subseteq \mathbb{R}^{d-1}$. As such, $f(\hat{y}_{k+j|k}) \leq P(E_{k+j}|y_0, \ldots, y_k)$ easily follows due to the fact that both expressions share a common integrand. It is therefore evident that our original claim $A_k^j \subseteq \Omega_{A_j}$, and thus $\bigcup_{j=1}^d A_k^j \subseteq \bigcup_{j=1}^d \Omega_{A_j}$ is mathematically sound.

According to this newly derived containment relationship, and by again using qualitative arguments, it is clear that the root-finding approximation will be more aggressive, and less optimistic than the closed form approximation. However, there is no containment relationship that can be established between the root-finding method and the exact optimal alarm region as could be performed for the closed form approximation. As such, even though the root-finding method incorporates all elements of the covariance matrix when computing its asymptotes, this approximation strategy may be overly aggressive and overshoot the performance of the exact optimal method under certain circumstances. This mathematical intuition will be supported by demonstrating this effect with examples later in the results section.

C. Redline and Predictive Alarm Systems

The two baseline alarm systems mentioned previously (redline and predictive) will be compared to the optimal alarm system and its approximations. All methods will attempt to predict the level-crossing event defined by Eqn. 4. The redline alarm system attempts to define an envelope, $[-L_A, L_A]$, outside of which an alarm will be triggered to forewarn of the impending level-crossing event. The probabilities necessary to compute P_d and P_{fa} based upon Eqns. 33-34 for this alarm system are provided in Eqns. 56-59, where we re-define $A_k = \{|y_k| > L_A\}$, such that the alarm is based only on the current process value.

$$P(A_k) = P(|y_k| > L_A) \quad (56)$$

$$= 2\Phi\left(\frac{-L_A}{\sqrt{\mathbf{C}\mathbf{P}_{ss}^L\mathbf{C} + R}}\right) \quad (57)$$

$$P(C_k, A_k) = P(C_k) - P(A_k') + P(C_k', A_k') \quad (58)$$

$$P(C_k', A_k') = \int_{-L_A}^{L_A} \int_{-L}^{L} \cdots \int_{-L}^{L} \mathcal{N}(\mathbf{z}; \mu_{\mathbf{z}}, \Sigma_{\mathbf{z}}) d\mathbf{z} \quad (59)$$

where

$$\begin{aligned}
\mathbf{z} &\triangleq \begin{bmatrix} y_k \\ \mathbf{y}_d \end{bmatrix} \\
\mu_{\mathbf{z}} &\triangleq \begin{bmatrix} \mu_{y_k} \\ \mu_{\mathbf{y}_d} \end{bmatrix} = \mathbf{0}_{d+1} \\
\Sigma_{\mathbf{z}} &\approx \begin{cases} \mathbf{C}\mathbf{P}_{ss}^{L}\mathbf{C}^{\top} + R & \forall i = j \in [0,\ldots,d] \\ \mathbf{C}\mathbf{A}^{j-i}\mathbf{P}_{ss}^{L}\mathbf{C}^{\top} & \forall j > i \in [0,\ldots,d] \end{cases}
\end{aligned}$$

The "redline" alarm system is termed as such in order to indicate that a simple alarm level crossing is used to predict a second more critical level-crossing. In this case two levels are used, L as the failure threshold, and L_A as the design threshold. For reasons stated earlier, this alarm system would be superior to a redline system that uses only a single level L, even though predicted future process values are not used.

The "predictive" alarm system does incorporate the use of predicted future process values, and defines the same envelope, $[-L_A, L_A]$, outside of which an alarm will be triggered to forewarn of the impending level-crossing event. However, the alarm definition differs from the redline method, such that $A_k = \{|\hat{y}_{k+d|k}| > L_A\}$. The predicted future process value $\hat{y}_{k+d|k}$ is found from standard Kalman filter Eqn. 14. The probabilities necessary to compute P_d and P_{fa} based upon Eqns. 33-34 for this alarm system are provided in Eqns. 60-63.

$$\begin{aligned}
P(A_k) &= P(|\hat{y}_{k+d|k}| > L_A) && (60)\\
&= 2\Phi\left(\frac{-L_A}{\sqrt{\lambda_a}}\right) && (61)\\
P(C_k, A_k) &= P(C_k) - P(A'_k) + P(C'_k, A'_k) && (62)\\
P(C'_k, A'_k) &= \int_{-L}^{L}\cdots\int_{-L}^{L}\int_{-L_A}^{L_A}\mathcal{N}(\mathbf{z};\mu_{\mathbf{z}},\Sigma_{\mathbf{z}})d\mathbf{z} && (63)
\end{aligned}$$

where

$$\begin{aligned}
\mathbf{z} &\triangleq \begin{bmatrix} \mathbf{y}_d \\ \hat{y}_{k+d|k} \end{bmatrix} \\
\mu_{\mathbf{z}} &\triangleq \begin{bmatrix} \mu_{\mathbf{y}_d} \\ \mu_{\hat{y}_{k+d|k}} \end{bmatrix} = \mathbf{0}_{d+1} \\
\Sigma_{\mathbf{z}} &\triangleq \begin{bmatrix} \Sigma_{\mathbf{y}_d} & \Lambda_a^{\top} \\ \Lambda_a & \lambda_a \end{bmatrix} \\
\lambda_a &= \mathbf{C}\mathbf{A}^d(\mathbf{P}_{ss}^{L} - \hat{\mathbf{P}}_{ss}^{R})(\mathbf{A}^{\top})^d\mathbf{C}^{\top} \\
\Lambda_a &= \mathbf{C}\mathbf{A}^d(\mathbf{P}_{ss}^{L} - \hat{\mathbf{P}}_{ss}^{R})\mathbf{O}^{\top}
\end{aligned}$$

Note that λ_a and Λ_a have been derived with the aid of the projection theorem. All of the alarm systems described thus far will be compared using the area under the ROC curve (AUC). This provides a performance metric that characterizes the ability of each alarm system to accurately predict the level-crossing event. The AUC has been deemed as a theoretically valid metric for model selection and algorithmic comparison [19]. The parameters of interest are L_A for the redline and predictive methods, and P_b for the optimal alarm system and its approximations. Results will follow in the subsequent section.

IV. Example

The example to be used for the presentation of our results has no specific application, but is generic and based upon the same example used by Svensson [2]. The model parameters are provided in Eqns. 64-67.

$$\begin{aligned}
\mathbf{A} &= \begin{bmatrix} 0 & 1 \\ -0.9 & 1.8 \end{bmatrix} && (64)\\
\mathbf{C} &= \begin{bmatrix} 0.5 & 1 \end{bmatrix} && (65)\\
\mathbf{Q} &= \begin{bmatrix} 0 & 0 \\ 0 & 1 \end{bmatrix} && (66)\\
R &= 0.08 && (67)
\end{aligned}$$

Unless otherwise stated, all cases to be compared will use a threshold of $L = 16$ while varying d, or a prediction window of $d = 5$ while varying L.

V. Results & Discussion

A comparison of the AUC for all alarm systems for a prediction window of $d = 5$ while varying $L \in [2.89, 17.83]$ is shown in Fig. 6.

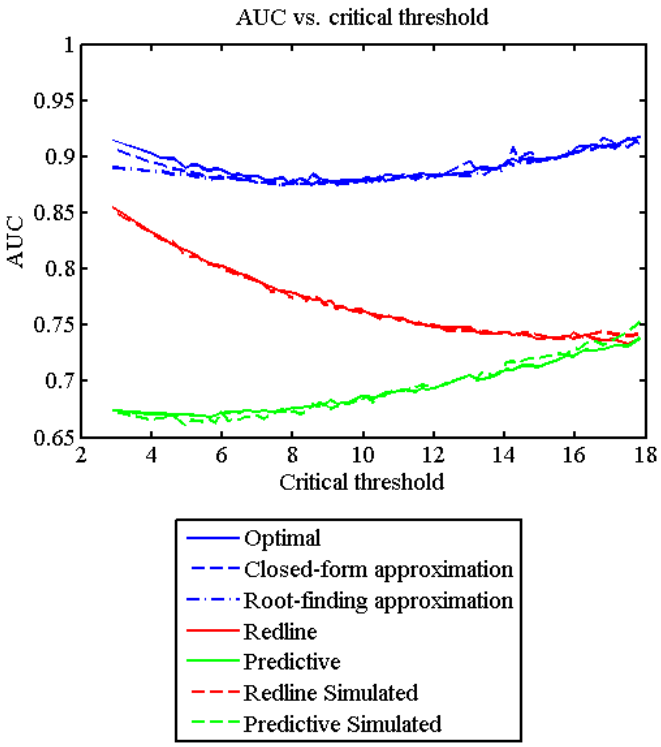

Fig. 6. AUC for all alarm systems a function of critical threshold, L

It is very clear that the optimal alarm system and its approximations outperform the redline and predictive methods, over the entire range of values shown for L, as expected. Another important point to note is that the approximations shown as dashed and dash-dotted blue lines, approximate the exact optimal performance (in solid blue) quite well over most of the range of values shown for L. However, as $L \to 0$,

the approximation breaks down as evidenced by the notable divergence of AUC values. More careful analysis of the reasons for this divergence, including its relation to the design parameter P_b will be presented subsequently.

The ROC curves for the exact optimal alarm system were computed using the Monte-Carlo style simulation described earlier, and based upon a computationally efficient method documented by Fawcett [20]. The corresponding AUC values were computed using a trapezoidal integration method presented by Bradley [19]. The same simulation-based method for generating ROC curve statistics and subsequently the AUC value can be used for both the redline and predictive methods, as shown in Fig. 6.

The ROC curve statistics for both approximations to the optimal alarm system were generated by the use of Eqns. 33-34, as were the redline and predictive alarm systems. The latter were verified by comparison to the corresponding simulation-based AUC values, which matched quite well. The use of Genz's [17] numerical integration technique to compute the probabilities given in Eqns. 33-34 are inherently based upon Monte Carlo sampling. As such, a fixed number of random samples must be chosen to guide the resolution for all integrations. All of the results presented in this article use 3600 as the number of random samples for each integration performed.

The ROC curve statistics in this case were computed in a different manner than their simulation-based counterparts. The design parameters of interest, L_A or P_b were varied over their feasible ranges in an adaptive pointwise manner in order to construct ROC curves that targeted a fixed resolution. However, the AUC values were still computed based upon the same trapezoidal integration methods presented by Bradley [19] as before.

It is necessary to ensure that the smoothness of the ROC curves and AUC curve as a function of L constructed by using these different methods are comparable. We appeal to use of the standard error to reconcile the contrasting magnitudes of error introduced. It is well known that the Hanley-McNeil method [19] for estimating the standard error of the AUC yields confidence bounds that are often too conservative and excessively wide. As such, a bootstrap resampling method was used to form confidence bounds for the AUC values resulting from the application of Eqns. 33-34 to construct corresponding ROC curves.

The resulting $SE(AUC)$ values were then subsequently used to guide establishing a partial termination criterion for the ROC curves constructed via simulation. This provides some assurance that the smoothness of the ROC and AUC curves using the two different methods are comparable. An additional termination criterion to complement the $SE(AUC)$ value criterion is to use the fixed resolution targeted for construction of the ROC curve as before. Since we now have some assurance of comparability of smoothness of the AUC curve and resolution of the ROC curve, the issue of computational complexity can be addressed. Table II provides a summary of the empirically generated timing tests which illustrate both off-line design-time and on-line run-time computational complexity.

TABLE II
EMPIRICAL ANALYSIS OF COMPUTATIONAL COMPLEXITY

	Mean Design-Time	Mean Run-Time
Optimal	81 min	9.5 msec
Closed-form	48.5 sec	0.15 msec
Root-finding	57.3 sec	0.12 msec

The second column of Table II includes the mean design time of both the redline and predictive alarm systems as well as the optimal system or its approximations across all values of L. Clearly, there is an order of magnitude greater computational burden by using the simulation-based method of designing alarm systems. Also, as expected the mean design-time for the root-finding approximation exceeds that of the closed-form approximation. As is clear by Fig. 6, there is no great loss in accuracy by using these approximations except for small values of L, where there is a perceptible, but perhaps still negligible loss.

The third column of Table II provides the mean run-time across all values of L, where it is evident again that the computational requirements of the optimal alarm condition exceed those of its approximations. In this case, the approximations involve only the time for limit checking of the type governed by Eqn. 45. Thus the actual time for root-finding is not included in the reported time for that approximation as shown in Table II, which might account for the fact that it is on par with the time for the closed form approximation. The mean run-time for checking the exact optimal alarm condition is based upon computing Eqns. 22-23, which naturally requires more time than a simple limit check.

Note that we have summarized these empirical complexity results in a tabular rather a graphical fashion, aggregating the results by taking the mean over all values of L. The main reason for doing so is that there is no perceptible trend across L for any of the cases, with the possible exception of the design time for both the closed form and root finding approximations. For these exceptions, there is a general upward trend of the design time (which again include design times for both the redline and predictive alarm systems) as L increases. This effect is intuitive because it becomes more difficult to construct an ROC curve for low probability events (higher L) that have the same target resolution as higher probability events (lower L), when employing numerical integration.

It is also of interest to investigate the case when using a fixed threshold of $L = 16$ while varying $d \in [2, \ldots, 24]$. A comparison of the AUC for all alarm systems for this case is shown in Fig. 7. As is clear from Fig. 7 and corroborated by Fig. 6, the optimal alarm system and its approximations outperform the redline and predictive methods as before, this time over the entire range of values shown for d. Furthermore, as the prediction window increases, the predictive performance as characterized by the AUC decreases for all alarm systems, as is to be expected. A more detailed study on the limiting effects of AUC as $d \to \infty$ will be conducted in a sequel article. Due to the use of a modestly large fixed threshold of $L = 16$ however, there are no deleterious effects as a result

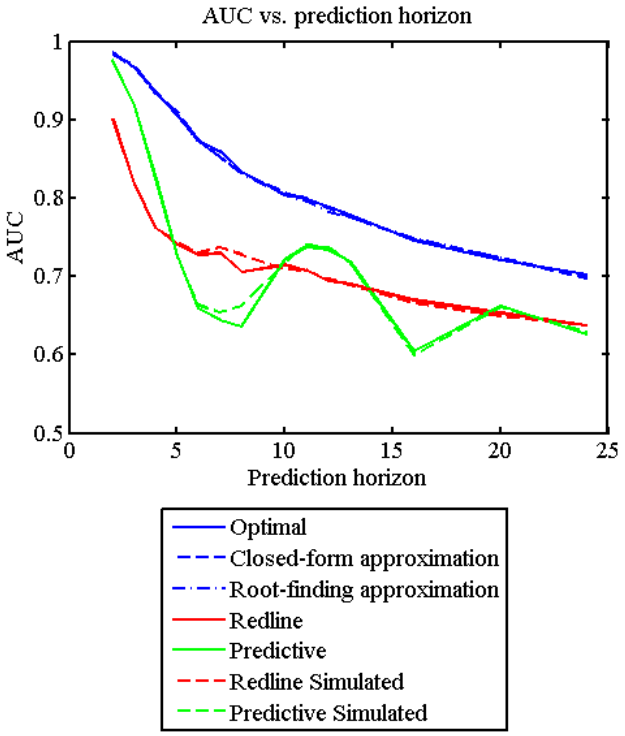

Fig. 7. AUC for all alarm systems as a function of prediction window, d

of using approximations to the optimal alarm system as were found when investigating the case when varying L to small values.

Characterization of complexity as d increases is also of interest. For the most part, the results are very similar to what was presented in Table II for the case in which a prediction window of $d = 5$ was used while varying L. Specifically, the mean design time for the exact optimal alarm system (along with redline and predictive alarm systems) was on par with what was shown in Table II (74 min in lieu of 81 min). However, the run-time in this case increases linearly as shown in Fig. 8.

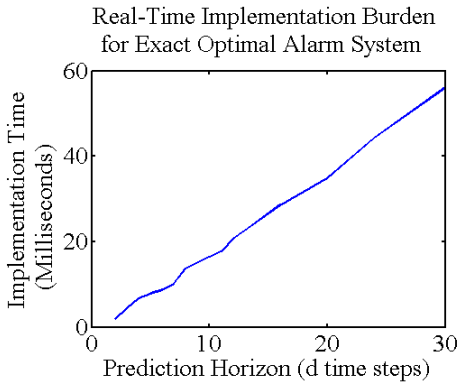

Fig. 8. Empirical run-time complexity as a function of prediction window

As the prediction window increases, the runtime for checking the exact optimal alarm condition based upon computing Eqns. 22-23 naturally requires more time for larger prediction horizons. A key advantage in using approximations can therefore be realized. For both the closed form and root finding approximations, the mean runtime is exactly on par with what was presented in Table II for the case in which a prediction window of $d = 5$ was used while varying L (averaging 0.11 msec). This is primarily due to the fact that, again, runtime for the approximations involve only limit checking of the type governed by Eqn. 45.

As for the design time of the approximations, they too exhibit similar characteristics to what was presented and discussed in conjunction with Table II. Specifically, there is a general upward trend of the design time (which again include design times for both the redline and predictive alarm systems) as d increases. The mean design times are moderately higher than what was presented in Table II (111 sec in lieu of 44.2 sec for the closed-form approximation and 129 sec in lieu of 55.2 sec for the root-finding approximation).

Now we return to addressing the issue of the limitations of using the optimal alarm approximations, which break down as $L \rightarrow 0$. A notable divergence of AUC values was evident in Fig. 6 under this condition. We may gain insight into the reasons for this divergence by examining a candidate ROC curve corresponding to a small value of L. In Fig. 9, we can visually discern how both approximations break down as related to the design parameter P_b for a small value of $L \approx 4$ compared to a larger value of $L \approx 10$.

There are many observations which can be made about Fig. 9. The topmost panels of the figure illustrate ROC curves corresponding to the different values of L. It is clear that appealing to different methods of constructing the ROC curves for the predictive and redline optimal alarm systems yield almost identical results. This also serves to verify the correctness and equivalence of using either method of ROC curve construction for these alarm systems. They manifest a reasonably similar level of resolution and smoothness due to proper choice of termination criteria.

However, for the optimal alarm system in solid blue, the two approximations shown as dashed and doted blue lines yield ROC curves that are close but not identical to the exact optimal result when $L \approx 4$. On the top right panel when $L \approx 10$, the ROC curve approximations appear to be much closer than on the top left panel where $L \approx 4$. This substantiates a previous observation made from Fig. 6, that as L decreases, the approximation loses its accuracy. Furthermore, from the previous section, Figs. 2 and 5 showed the optimal alarm regions and their approximations to provide further evidence of this loss of accuracy as L decreases. Those figures were based upon the same example used to generate the results presented in this section.

Further insight can be gained by inspecting the bottom two panels of Fig. 9 as well. Note that the bottom panels show the missed detection and false positive rates as a function of P_b. The complement of the former is the true positive rate, which along with the false positive rate, is used to construct the ROC curves shown on the top panels. There are a few important observations to be made in regards to these bottom panels. First, the closed form approximations to the

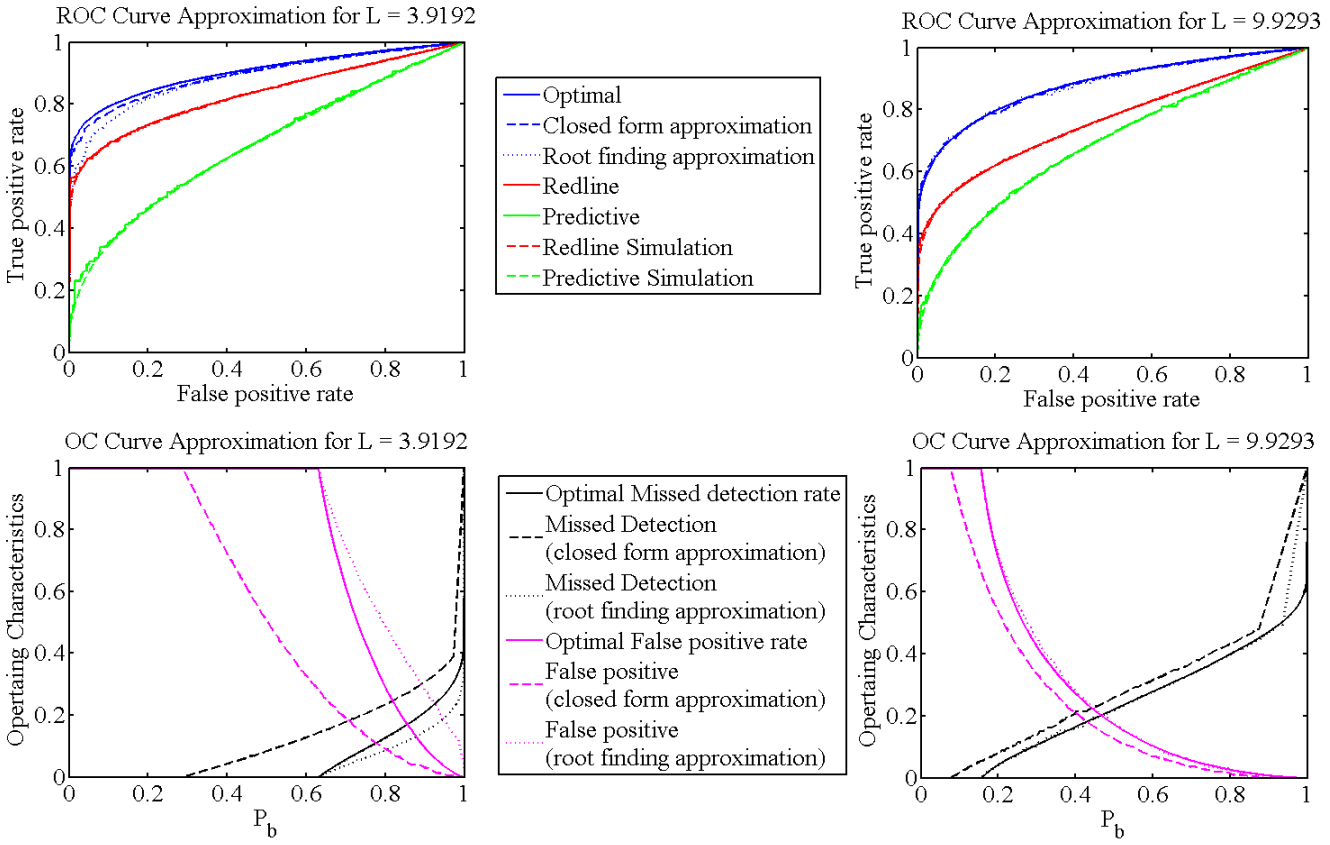

Fig. 9. ROC Curves and supporting statistics for all alarm systems, demonstrating negligible loss in accuracy for both approximations, and superiority of root-finding approximation over closed-form approximation

optimal alarm system yield true and false positive rates that are systematically underreported for both values of L shown. This corroborates the mathematical observation made from the previous section based upon the containment relationship of the closed form approximation to the exact optimal alarm region, $\bigcup_{j=1}^{d}\bigcup_{i\in\mathcal{B}} A_k^{i,j} \subseteq \bigcup_{j=1}^{d} A_k^j \subseteq A_k$. For the smaller value of $L \approx 4$, this underreporting of the true and false positive rates is even more striking than for the larger value of $L \approx 10$.

Furthermore, the root finding approximations to the optimal alarm system yield true and false positive rates that are overreported for both values of L shown. This is much more clear for the smaller value of $L \approx 4$ than for the larger value of $L \approx 10$. Hence, again this corroborates an inference made from mathematical observations made in the previous section. Recall the containment relationship between the root finding and closed form approximation to the exact optimal alarm region $\bigcup_{j=1}^{d} A_k^j \subseteq \bigcup_{j=1}^{d} \Omega_{A_j}$. It was suggested that the root finding approximation strategy may be overly aggressive and overshoot the performance of the exact optimal method under certain circumstances. This is clear for the smaller value of $L \approx 4$.

There is one last important note about the root finding approximations that is evident in the bottom two panels of Fig. 9. The feasible range of values for P_b is identical to the exact optimal alarm region of feasibility, which was also proven mathematically in the previous section. The same is not true for the closed form approximation, where the region of feasibility is clearly different, and drastically so for the smaller value of $L \approx 4$.

Finally, it is evident that the underreporting of true and false positive rates as demonstrated in the bottom two panels of Fig. 9 does not translate to the same visually striking disparities for the ROC curves on the top two panels. These striking disparities are obfuscated by the fact that the ROC curve is a parametric function of the design parameter. As such, great caution should be taken when using the ROC curve as the sole basis for the design of alarm systems based up the given approximations. Specific criteria for the design of an alarm system based upon provisions for maximum allowable false positive or missed detection rates may be given. With these constraints, the supporting statistics as shown on the bottom panels of Fig. 9 should be used to complement design based upon the ROC curve.

VI. Conclusions & Future Work

In this article we have introduced a novel state-space approach to the optimal alarm systems literature, and hope to have also participated in the Kalman filter-based fault detection literature discussion from a different theoretical angle as well.

In doing so, we have demonstrated that there is a negligible loss in overall accuracy when using approximations to the theoretically optimal predictor for a stationary linear Gaussian process, at the advantage of greatly reduced computational complexity. The negligibility of the loss in accuracy was demonstrated by comparing approximations to the optimal level-crossing predictor to two competing methods which were clearly outperformed over various ranges for both L and d. However, care should be taken when designing alarm systems for which level-crossing events are defined with small values of L. Specifically, when using approximations, alarm system design should be governed both by ROC curve analysis as well as supporting false positive or missed detection rate statistics parameterized by the design parameter P_b.

In future work, we will investigate limiting effects of AUC for the closed-form approximation introduced in this article. Specifically, limiting values for relevant statistics as P_b, L, R, and d approach the extremities of their feasible ranges will be examined. In doing so we hope to facilitate a new and broader context for the design of an optimal alarm system as related more to important engineering design parameters. Furthermore, we aim to the investigate control theoretic implications and ramifications of using the Kalman filter in tandem with optimal alarm theory that naturally follow. Here it will also be possible to gain further insight into important engineering design considerations for both the analysis and synthesis of algorithms used for mitigation of potential failures from a practical standpoint. Relaxing some of the inherent assumptions made in this article to the point where non-parametric methods such as particle filtering may also provide a natural vehicle for the extension of optimal alarm theory to other practical research domains. Finally, extension of this work to systems containing both multivariate inputs and outputs is important, and has practical appeal to the field of data mining. As such, scalability and complexity will remain important considerations.

VII. Acknowledgements

The author would like to acknowledge the guidance and advocacy of Prof. David Auslander of the Mechanical Engineering Department at the University of California, Berkeley, and Dr. Cliff Federspiel during the completion of his Ph.D. in conducting applied research related to this topic during its conception. However, continued research on the more theoretical aspects of this work would not have been possible without the support of the Integrated Vehicle Health Management (IVHM) project. The IVHM project is funded by the Aviation Safety Program of NASA's Aeronautics Research Mission Directorate. The author would also like to thank Dr. Mark Schwabacher, Dr. Nikunj Oza, Dawn McIntosh, John Wallerius, and Dr. Santanu Das for reviewing various versions of this article throughout its evolution. Finally, the author appreciates the important points made by the reviewers selected by the editorial board of the IEEE Transactions on Information Theory, whose valuable comments and criticism have greatly helped to allow for the development of a more technically sound article.

Appendix I
Theorems and Lemmas

Theorem 1: From Eqns. 1-3 it is clear that successive output values of the stationary stochastic process, y_k admit a well-defined jointly Gaussian probability density function. Also, the level-crossing event, C_k, defined through Eqn. 4, represents at least one exceedance outside of the threshold envelope specified by $[-L, L]$ of the process y_k. Then the optimal level-crossing predictor can be written as $P(C_k|y_0, \ldots, y_k) \geq P_b$, where the condition for optimality is as specified and defined by the use of the likelihood ratio criterion, shown in Eqn. 68 as a result of the Neyman-Pearson Lemma, shown by DeMaré [5], and more explicitly by Lindgren [6],[21].

$$\frac{p(y_0, \ldots, y_k|C_k^{'})}{p(y_0, \ldots, y_k|C_k)} \leq \lambda \tag{68}$$

Proof: Using Lemma 1 (which curiously appears very much like Bayes' rule, but can be distinguished from it due to the use of both probabilities and density functions), we can rewrite Eqn. 68 as follows:

$$\begin{aligned}
\frac{p(y_0, \ldots, y_k|C_k^{'})}{p(y_0, \ldots, y_k|C_k)} &\leq \lambda \\
\frac{\frac{P(C_k^{'}|y_0,\ldots,y_k)\cancel{p(y_0,\ldots,y_k)}}{P(C_k^{'})}}{\frac{P(C_k|y_0,\ldots,y_k)\cancel{p(y_0,\ldots,y_k)}}{P(C_k)}} &\leq \lambda \\
\frac{P(C_k^{'}|y_0, \ldots, y_k)P(C_k)}{P(C_k|y_0, \ldots, y_k)P(C_k^{'})} &\leq \lambda
\end{aligned}$$

However, due to the assumption of stationarity of the process, the size of the alarm region, $P(C_k)$, associated with the uniformly most powerful test of the hypothesis $\mathcal{H}_0$ is by definition a constant value. The hypothesis being tested in this case is of the level-crossing event, C_k. Due to the size of alarm region being fixed, we can define new constants as shown below.

$$\begin{aligned}
\frac{1 - P(C_k|y_0, \ldots, y_k)}{P(C_k|y_0, \ldots, y_k)} &\leq \lambda\frac{P(C_k^{'})}{P(C_k)} \triangleq \gamma \\
P(C_k|y_0, \ldots, y_k) &\geq \frac{1}{1+\gamma} \triangleq P_b \\
\Leftrightarrow P(C_k|y_0, \ldots, y_k) &\geq P_b
\end{aligned}$$

■

Lemma 1:

$$p(y_0, \ldots, y_k|C_k) = \frac{P(C_k|y_0, \ldots, y_k)p(y_0, \ldots, y_k)}{P(C_k)} \tag{69}$$

Proof:

$$\begin{aligned}
p(y_0, \ldots, y_k|C_k) &\triangleq \frac{\int \cdots \int_{\Omega_C} p(y_0, \ldots, y_{k+d})d\mathbf{y}_d}{P(C_k)} \\
&= \frac{\int \cdots \int_{\Omega_C} p(y_0, \ldots, y_{k+d})d\mathbf{y}_d}{p(y_0, \ldots, y_k)} \\
&\quad \cdot \frac{p(y_0, \ldots, y_k)}{P(C_k)} \\
&= \frac{P(C_k|y_0, \ldots, y_k)p(y_0, \ldots, y_k)}{P(C_k)}
\end{aligned}$$

where by definition $P(C_k|y_0,\ldots,y_k)\stackrel{\triangle}{=}$

$$\begin{aligned} & \int\cdots\int_{\Omega_C} p(y_{k+1},\ldots,y_{k+d}|y_0,\ldots,y_k)d\mathbf{y}_d \\ = & \frac{\int\cdots\int_{\Omega_C} p(y_0,\ldots,y_{k+d})d\mathbf{y}_d}{p(y_0,\ldots,y_k)} \\ \text{and } \Omega_C = & \{\mathbf{y}_d\in\mathbb{R}^d : C_k\stackrel{\triangle}{=}\bigcup_{j=1}^{d} S_{k+j}\} \end{aligned}$$

■

Lemma 2:

$$\begin{gathered} P_{b_d}=\max_j P_{b_j} \\ \Updownarrow \\ V_{k+j+1|k}>V_{k+j|k},\quad \forall j\in[1,\ldots,d] \end{gathered}$$

Proof: The posited claim is true *iff*

$$P_{b_1}<\ldots<P_{b_j}<P_{b_{j+1}}<\ldots<P_{b_d}$$

More compactly,

$$P_{b_j}<P_{b_{j+1}},\quad \forall j\in[1,\ldots,d]$$

The following chain of inequalities is true $\forall j\in[1,\ldots,d]$.

$$\begin{aligned} P_{b_j} &< P_{b_{j+1}} \\ \Phi^{-1}(P_{b_j}) &< \Phi^{-1}(P_{b_{j+1}}) \\ \left(\frac{-L}{\Phi^{-1}(P_{b_{j+1}})}\right)^2 &> \left(\frac{-L}{\Phi^{-1}(P_{b_j})}\right)^2 \\ V_{k+j+1|k} &> V_{k+j|k} \end{aligned}$$

■

Lemma 3:

$$\begin{gathered} \mathbf{P}^R_{ss}\succeq\hat{\mathbf{P}}^R_{ss} \\ \Downarrow \\ V_{k+j+1|k}>V_{k+j|k},\quad \forall j\in[1,\ldots,d] \end{gathered}$$

Proof:

$$\begin{aligned} \mathbf{P}^R_{ss} &\succeq \hat{\mathbf{P}}^R_{ss} \\ \mathbf{P}^R_{ss}-\hat{\mathbf{P}}^R_{ss} &\succeq 0 \\ \mathbf{x}^\top(\mathbf{P}^R_{ss}-\hat{\mathbf{P}}^R_{ss})\mathbf{x} &\geq 0,\quad \forall\mathbf{x}\in\mathbb{R}^n \\ \mathbf{x}^\top(\hat{\mathbf{P}}^R_{ss}+\mathbf{Q}-\mathbf{P}^R_{ss})\mathbf{x} &\leq \mathbf{x}^\top\mathbf{Q}\mathbf{x},\quad \forall\mathbf{x}\in\mathbb{R}^n \end{aligned}$$

By using the steady-state version of Eqn. 12 and the discrete algebraic Lyapunov equation we now have the following, $\forall\mathbf{x}\in\mathbb{R}^n$.

$$\begin{aligned} \mathbf{x}^\top(\hat{\mathbf{P}}^R_{ss}-\mathbf{A}\hat{\mathbf{P}}^R_{ss}\mathbf{A}^\top)\mathbf{x} &\leq \mathbf{x}^\top(\mathbf{P}^L_{ss}-\mathbf{A}\mathbf{P}^L_{ss}\mathbf{A}^\top)\mathbf{x} \\ \mathbf{x}^\top(\hat{\mathbf{P}}^R_{ss}-\mathbf{P}^L_{ss})\mathbf{x} &\leq \mathbf{x}^\top\mathbf{A}(\hat{\mathbf{P}}^R_{ss}-\mathbf{P}^L_{ss})\mathbf{A}^\top\mathbf{x} \end{aligned}$$

Let $\mathbf{x}^\top\stackrel{\triangle}{=}\mathbf{C}\mathbf{A}^j,\quad \forall j\in[1,\ldots,d]$, and add $\mathbf{C}\mathbf{P}^L_{ss}\mathbf{C}^\top+R$ to both sides of the inequality above. It then follows that the following relations hold true, $\forall j\in[1,\ldots,d]$.

$$\begin{aligned} \mathbf{C}\mathbf{P}_{k+j|k}\mathbf{C}^\top+R &\leq \mathbf{C}\mathbf{P}_{k+j+1|k}\mathbf{C}^\top+R \\ V_{k+j+1|k} &> V_{k+j|k} \end{aligned}$$

■

Lemma 4: $R>0\Rightarrow\mathbf{P}^R_{ss}\succeq\hat{\mathbf{P}}^R_{ss}$

Proof: It is true that

$$R>0\Leftrightarrow R^{-1}>0$$

Under the condition that $\mathbf{C}\in\mathbb{R}^{1\times n}$, where $n>1$, with no rank condition on $\mathbf{C}$, Lemma 5 can be used to support the following implication:

$$R^{-1}>0\Rightarrow\mathbf{C}^TR^{-1}\mathbf{C}\succeq 0$$

Also, given the matrix inversion lemma applied to Eqn. 19 shown below, the subsequent series of equations proves that $\mathbf{P}^R_{ss}\succeq\hat{\mathbf{P}}^R_{ss}$.

$$\begin{aligned} \hat{\mathbf{P}}^R_{ss} &= \mathbf{P}^R_{ss}-\mathbf{P}^R_{ss}\mathbf{C}^T(\mathbf{C}\mathbf{P}^R_{ss}\mathbf{C}^T+R)^{-1}\mathbf{C}\mathbf{P}^R_{ss} \\ &\stackrel{M.I.L}{=} \left[(\mathbf{P}^R_{ss})^{-1}+\mathbf{C}^TR^{-1}\mathbf{C}\right]^{-1} \\ \therefore(\hat{\mathbf{P}}^R_{ss})^{-1} &= (\mathbf{P}^R_{ss})^{-1}+\mathbf{C}^TR^{-1}\mathbf{C} \end{aligned}$$

$$\begin{aligned} \mathbf{C}^TR^{-1}\mathbf{C} &\succeq 0 \\ (\hat{\mathbf{P}}^R_{ss})^{-1}-(\mathbf{P}^R_{ss})^{-1} &\succeq 0 \\ (\hat{\mathbf{P}}^R_{ss})^{-1} &\succeq (\mathbf{P}^R_{ss})^{-1} \\ \mathbf{P}^R_{ss} &\succeq \hat{\mathbf{P}}^R_{ss} \end{aligned}$$

■

Lemma 5: Given $\mathbf{L}\in\mathbb{R}^{n\times d}$, for which $d>n$ and there exists no rank condition on $\mathbf{L}$: $\mathbf{M}\succ 0\Rightarrow\mathbf{L}^T\mathbf{M}\mathbf{L}\succeq 0$

Proof:

$$\begin{aligned} \mathbf{M} &\succeq 0 \\ \therefore\mathbf{x}^T\mathbf{M}\mathbf{x} &\geq 0,\forall\mathbf{x}\in\mathbb{R}^n \\ \mathbf{x} &\stackrel{\triangle}{=} \mathbf{L}\mathbf{y} \\ Null(\mathbf{L}) &\stackrel{\triangle}{=} \{\mathbf{y}:\mathbf{L}\mathbf{y}=0\} \\ \dim Null(\mathbf{L}) &\geq d-n>0 \\ \exists\mathbf{y} &: \mathbf{L}\mathbf{y}=0 \\ \mathbf{y}^T\mathbf{L}^T\mathbf{M}\mathbf{L}\mathbf{y} &\geq 0,\forall\mathbf{x}\in\mathbb{R}^n \\ \mathbf{L}^T\mathbf{M}\mathbf{L} &\succeq 0 \end{aligned}$$

■

REFERENCES

[1] A. Svensson, "Event prediction and bootstrap in time series," Ph.D. dissertation, Lund Institute of Technology, September 1998.

[2] A. Svensson, J. Holst, R. Lindquist, and G. Lindgren, "Optimal prediction of catastrophes in autoregressive moving-average processes," *Journal of Time Series Analysis*, vol. 17, no. 5, pp. 511–531, 1996.

[3] R. A. Martin, "Optimal prediction, alarm, and control in buildings using thermal sensation complaints," Ph.D. dissertation, University of California, Berkeley, 2004.

[4] S.-I. Beckman, J. Holst, and G. Lindgren, "Alarm characteristics for a flood warning system with deterministic components," *Journal of Time Series Analysis*, vol. 11, no. 1, pp. 1–18, March 1987.

[5] J. DeMaré, "Optimal prediction of catastrophes with application to Gaussian processes," *Annals of Probability*, vol. 8, no. 4, pp. 840–850, August 1980.

[6] G. Lindgren, "Optimal prediction of level crossings in Gaussian processes and sequences," *Annals of Probability*, vol. 13, no. 3, pp. 804–824, August 1985.

[7] A. J. Rainal, "Zero-crossing principle for detecting narrow-band signals," *IEEE Transactions on Instrumentation and Measurement*, vol. IM-15, no. 1-2, pp. 38–43, 1966.
[8] T. H. Kerr, "False alarm and correct detection probabilities over a time interval for restricted classes of failure detection algorithms," *IEEE Transactions on Information Theory*, vol. IT-28, no. 4, pp. 619–631, July 1982.
[9] J. P. Butas, L. M. Santi, and R. B. Aguilar, "A tiered approach to J-2X health and status monitoring," in *Proceedings of the 54th Joint Army-Navy-NASA-Air Force Propulsion Meeting*, 2007.
[10] A. S. Willsky and H. L. Jones, "A generalized likelihood ratio approach to the detection and estimation of jumps in linear systems," *IEEE Transactions on Automatic Control*, vol. 21, no. 1, pp. 108–112, 1976.
[11] F. Gustafson, "The marginalized likelihood ratio test for detecting abrupt changes," *IEEE Transactions on Automatic Control*, vol. 41, no. 1, pp. 66–78, 1996.
[12] D. J. Pedregal and M. C. Carnero, "State space models for condition monitoring: a case study," *Reliability Engineering & System Safety*, vol. 91, no. 2, pp. 171 – 180, 2006, selected Papers Presented at QUALITA 2003.
[13] M. Antunes, A. A. Turkman, and K. F. Turkman, "A Bayesian approach to event prediction," *Journal of Time Series Analysis*, vol. 24, no. 6, pp. 631–646, November 2003.
[14] T. H. K. III, "Drawbacks of residual-based event detectors like GLR or IMM filters in practical situations," *IEEE Transactions on Signal Processing (preprint)*, 2006.
[15] N. H. Pontoppidan and J. Larsen, "Unsupervised condition change detection in large diesel engines," in *Proceedings of the 13th IEEE Workshop on Neural Networks for Signal Processing*. IEEE Press, September 2003, pp. 565–574.
[16] F. Lewis, *Applied Optimal Control & Estimation: Digital Design & Implementation*. Prentice Hall, Inc., 1992.
[17] A. Genz, "Numerical computation of multivariate normal probabilities," *Journal of Computational and Graphical Statistics*, vol. 1, pp. 141–149, 1992.
[18] T. H. K. III, "Integral evaluations enabling performance tradeoffs for two-confidence-region-based failure detection," *Journal of Guidance, Control, and Dynamics*, vol. 29, no. 3, pp. 757–762, May–June 2006.
[19] A. P. Bradley, "The use of the area under the ROC curve in the evaluation of machine learning algorithms," *Pattern Recognition*, vol. 30, no. 7, pp. 1145 – 1159, 1997.
[20] T. Fawcett, "ROC graphs: Notes and practical considerations for data mining researchers," Hewlett Packard Laboratories, Technical Report HPL-2003-4, 2003.
[21] G. Lindgren, "Model processes in nonlinear prediction with application to detection and alarm," *Annals of Probability*, vol. 8, no. 4, pp. 775–792, August 1980.